Electric-Field-Induced Coherent Anti-Stokes Raman Scattering of Hydrogen Molecules in Visible Region for Sensitive Field Measurement

Takeru Koike, Hitoshi Muneoka, Kazuo Terashima, and Tsuyohito Ito*
Department of Advanced Materials Science, Graduate School of Frontier Sciences, The University of Tokyo, 5-1-5 Kashiwanoha, Kashiwa, Chiba 277-8561, Japan

(Received 2 December 2021; revised 24 May 2022; accepted 3 June 2022; published 13 July 2022)

Nonintrusive optical measuring of electric fields in space is crucial for various sciences and technologies. In this study, a simple and highly sensitive optical electric field measurement is demonstrated in high-pressure hydrogen by performing electric-field-induced coherent anti-Stokes Raman scattering (E-CARS) in the visible region. The minimum detectable electric field is 0.5 V/mm at atmospheric pressure. This method does not require excited or atomic species and shows a considerably higher sensitivity than those demonstrated by the commonly applied E-CARS method in the infrared region and electric-field-induced second-harmonic generation. This method can be applied to various Raman-active molecules.

DOI: 10.1103/PhysRevLett.129.033202

An electric field is one of the basic parameters that describes various spaces, and nonintrusive measurement of electric fields is crucial in various fields and applications, such as atmospheric science [1,2], lightning or thunderstorm predictions [3], static electricity detection [4,5], and discharge and plasma physics [6–19]. Numerous optical methods are used to keep the disturbance of the system at a low level for electric field measurements in low-pressure environments [11,13] and/or environments that consist of excited or atomic species, which are products of plasma and discharge [8,9,12,17]; however, the methods suitable for high-pressure environments, especially without plasma and discharge generation, are limited. Two currently popular methods at near-atmospheric pressure without plasma and discharge generation are electric-field-induced coherent anti-Stokes Raman scattering (E-CARS) in the infrared region (E-CARSi) [6] and electric-field-induced second-harmonic generation (E-FISH) [20]. Since both methods produce a coherent beam as a signal, they are applicable for remote sensing of electric fields.

E-CARS and E-FISH are both third-order nonlinear optical effects. Their intensities are described according to the following expression [21,22]:

$$I^{(3)} \propto |\chi^{(3)}|^2 C_l E^2 I_1 I_2; \quad \chi^{(3)} \propto N, \tag{1}$$

where $I^{(3)}$ is the intensity of the induced light from the third-order nonlinear optical effect, $\chi^{(3)}$ is the third-order nonlinear susceptibility, C_l is a constant regarding the interaction lengths decided by the geometry and the phase-matching condition discussed later, and N is the number density of the molecules for E-FISH or the density difference of molecules at the lower and higher states involved in the Raman transition for E-CARS. E is the electric field strength applied to the targeted molecules, and I_1 and I_2 are the intensities of the incident laser beams. Two laser beams are usually used in the E-CARSi method so that the energy difference of the lasers matches the Raman-transition energy, where, under normal conditions, $I_1 \neq I_2$. To achieve the best phase-matching condition, the laser beams need to be aligned collinearly. In contrast, for simplicity, only one laser beam is used in the E-FISH method, and therefore, the condition $I_1 = I_2$ holds true. The equation shows that $I^{(3)}$ is proportional to N^2, thus, making both methods suitable for high-density environments such as atmospheric-pressure gases and liquids.

The schematics of the optical transitions of E-CARSi or E-FISH are shown in Fig. 1. A scheme of the conventional CARS is also shown in Fig. 1(b), since it is also generated independently of the electric field strength, and the CARS signal is applied in the analysis. In the E-FISH method [Fig. 1(a)], a laser beam of frequency ω is irradiated into the measurement region, and a beam corresponding to the second-harmonic signal of the frequency 2ω, whose

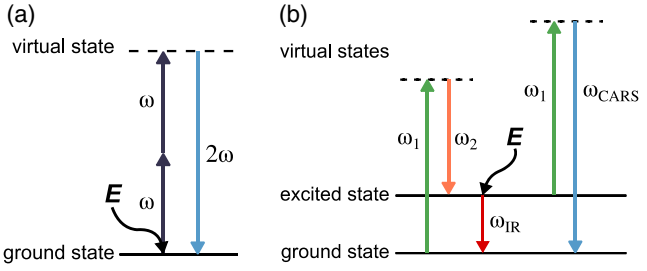

FIG. 1. Schematics of optical energy transitions. (a) Electric-field-induced second-harmonic generation. (b) Electric-field-induced coherent anti-Stokes Raman scattering in infrared region together with conventional CARS.

intensity is proportional to the square of the applied electric field strength, is generated. By selecting the appropriate laser wavelength, visible signals can be acquired, and a highly sensitive photodetector, such as a photomultiplier tube, can be employed to detect the E-FISH signal. As this technique does not require any resonance, it is capable of measuring the electric field almost independently of the molecular species of the gases. However, it is necessary to irradiate a relatively high-peak-intensity laser pulse to obtain sufficient signal intensity, often requiring femtosecond or picosecond laser irradiations [18,20]. On the other hand, when two laser beams at frequencies ω_1 and ω_2, whose energy difference matches the Raman-active vibrational transition energy in the medium, are irradiated, a conventional CARS beam at $\omega_{\mathrm{CARS}} = 2\omega_1 - \omega_2$ is generated, and the E-CARSi beam at $\omega_{\mathrm{IR}} = \omega_1 - \omega_2$ is induced additionally with an electric field in the E-CARSi method [Fig. 1(b)]. The intensity of the E-CARSi method is proportional to the square of the applied electric field strength, whereas the conventional CARS intensity does not depend on the field strength. Because both intensities are proportional to the square of the molecular density, by taking the ratio of the beam intensities of E-CARSi to CARS, part of the molecular density is canceled, and electric field measurements can be performed even without knowing the molecular density. Additionally, since this technique utilizes resonance with the Raman-transition energy of the targeted molecules, it is capable of measuring the sensitive electric field owing to $\chi^{(3)}$ and the conversion efficiencies being substantially higher than those in nonresonant processes [23,24]. However, E-CARSi, which corresponds to the Raman-transition energy, is in the infrared region in most cases, e.g., wavelengths at 2.4 [6] and 4.29 μm [22] in hydrogen and nitrogen, respectively, which prevents us from achieving highly sensitive field measurements owing to the difficulty in detecting infrared light. For example, when a low-band-gap photodiode cryogenically cooled to reduce the Johnson-Nyquist noise is applied, thermal background radiation causes difficulties. As a result, the detection limit demonstrated by the E-CARSi method [6] is similar to that of the E-FISH method [18].

In this study, we apply a scheme to generate E-CARS in the visible region (E-CARSv) to achieve highly sensitive field measurements. A schematic of the optical transition is shown in Fig. 2. This scheme was first proposed by Buldakov *et al.* [25], but there are no practical implementations yet. In this scheme, two laser beams at ω_1 and ω_{IR} are employed to induce $\omega_{\mathrm{CARS}} = \omega_1 + \omega_{\mathrm{IR}}$ with an electric field. For hydrogen, the wavelength corresponding to ω_{IR} is 2.4 μm, and the detected signal is at 436 nm (ω_{CARS}) when 532 nm is applied for ω_1. This method does not use any excited states of molecules; therefore, it can be applied to nondischarge media.

A schematic of the experimental setup is shown in Fig. 3. A seeded Nd:YAG laser beam at 1064 nm (Continuum

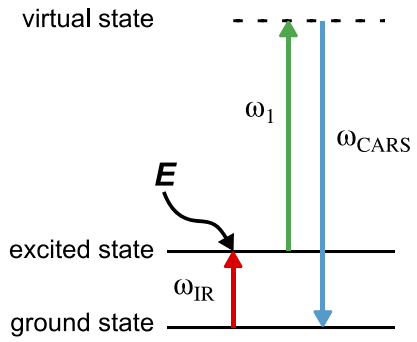

FIG. 2. Schematic of the optical energy transition for E-CARSv.

Surelite III-10JS) was converted into two beams at 532 nm and 2.4 μm using an optical parametric oscillator (OPO) and optical parametric amplifier (OPA) system and frequency-doubling crystals (Laser Vision, custom). The frequency of 2.4 μm corresponds to the Raman-active transition energy of the Q branch (vibrational quantum number $v = 0$ to 1) of the hydrogen molecule. The pulse durations of these beams were 3–5 ns, and their repetition rates were 10 Hz. The pulse powers were approximately 10 and 3 mJ for 532 nm and 2.4 μm, respectively. The polarization of both lasers is parallel to an externally applied electric field. Both lasers with their diameters of approximately 6 mm were collinearly aligned and focused on the center of the electrode gap in a hydrogen cell through a synthetic fused silica window by an off-axis parabolic mirror with a focal length of 75 mm. The beam diameters at the focal point were measured to be approximately 50 and 150 μm, and the peak irradiances were estimated to be

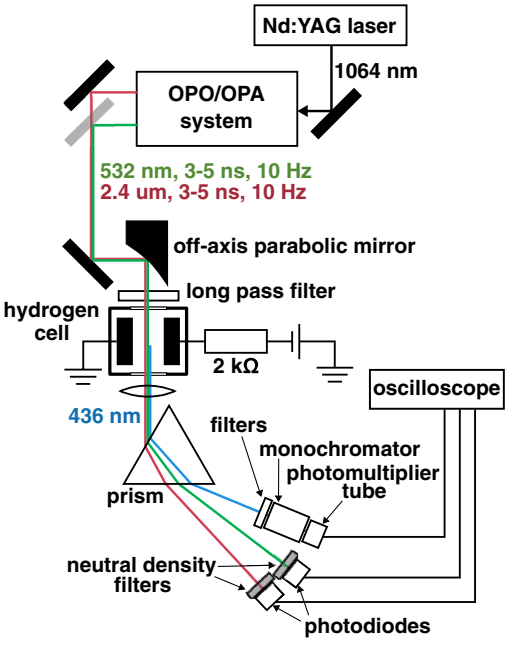

FIG. 3. Schematic of the experimental setup.

approximately 1 and 0.04 GW/mm^2 for 532 nm and 2.4 μm, respectively. A long pass filter was inserted before the window to cut off any sum-frequency light generated at the upstream optical components. Cylindrical stainless-steel flat-plate electrodes with a diameter of 17.0 mm were placed face to face with a gap distance of 3.5 mm to apply an electric field with a dc power supply. Because no discharge was generated under any experimental conditions, the electric field was simply calculated from the applied voltage and electrode gap. The voltage applied between the electrodes was measured with a voltmeter (FLUKE 175 true RMS multimeter) for voltages up to 45 V, or with a high-voltage probe (Tektronix P6015A) connected to a digital oscilloscope (Tektronix TDS744A) at a higher voltage. At the focal region, the beam at 436 nm was generated with an electric field, and three collinearly aligned beams emerged from the hydrogen cell through another synthetic fused silica window. Those three beams were separated by a prism, and the incident beams at 2.4 μm and 532 nm were monitored by photodetectors (Thorlabs PDA20H-EC and DET10A/M, respectively). The induced signal at 436 nm was detected by a photomultiplier tube (Hamamatsu Photonics R3896W) after an iris, short-pass filters, and a monochromator to reduce the stray light at 532 nm. All detected signals were recorded using a digital oscilloscope (Tektronix TDS5104B).

Figure 4 shows the result of the wavelength scan of the infrared laser around 2.4 μm. The applied electric field was

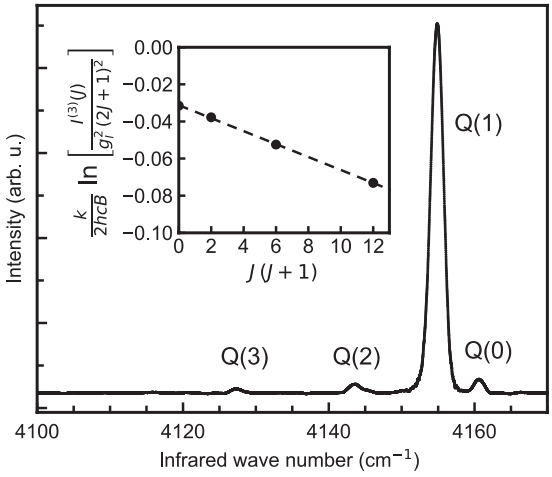

FIG. 4. E-CARSv spectrum under an atmospheric-pressure hydrogen environment with an applied electric field of 13 V/mm. The four observed peaks correspond to the Raman-transition energies of the Q branch of the hydrogen molecule. The inset is a Boltzmann plot for the rotational states J showing a rotational temperature of 286 K. The vertical axis of the inset is $(k/2hcB)\ln[I^{(3)}(J)/g_I^2(2J+1)]$, where k is Boltzmann's constant, h is Planck's constant, B is the rotational constant and is 60.853 cm^{-1} for hydrogen molecules, $I^{(3)}(J)$ is the intensity of each line, and g_I is the nuclear-spin degeneracy. The slope of the plot gives $-T_r^{-1}$.

13 V/mm, and the hydrogen pressure was 1 atm. The scanning speed of the infrared laser was approximately 0.07 cm^{-1}/s. Four peaks were observed at 4161, 4155, 4144, and 4127 cm^{-1}, which correspond to the rotational quantum numbers J of 0, 1, 2, and 3 in the Q branch ($v = 0$ to 1) of the hydrogen molecule, respectively. Similar to the conventional CARS spectra [26] at room temperature, the transition at 4155 cm^{-1} ($J = 1$) provides the strongest signal in the Q branch. The inset is the Boltzmann plot [27] indicating the rotational temperature T_r of 286 K, which is in good agreement with the room temperature of 290 K during the measurement. This agreement indicates that the laser irradiations did not disturb the temperature estimation in this study. While successful temperature estimations in ~1 atm environments were achieved with higher laser irradiances and powers [28,29], temperature elevation via laser pulses [30,31] should be carefully considered when the intense laser is applied. We attribute the observed linewidth of ~2 cm^{-1} (60 GHz) to the linewidth of the infrared laser since the linewidth of Raman spectra should be dominated by Doppler broadening, which is about 0.036 cm^{-1} (1.1 GHz) for 290 K hydrogen molecules. Together with the E-field dependence, it is clear that the signal in Fig. 4 was induced by the E-CARSv scheme. In the following measurements of the dependence of the electric field strength and molecular density, an infrared wave number of 4155 cm^{-1} was adopted.

The results of the signal intensity measurements in an atmospheric-pressure hydrogen environment as a function of the externally applied electric field strength are shown in Figs. 5(a) and 5(b), which show the results in the strong and weak electric field ranges, respectively. More than 1000 signals were averaged to reduce the effects of the shot-to-shot instability of the laser beams. Both results show the proportionality of the square root of the signal intensity to the electric field strength, as described in Eq. (1). This result for E-CARSv thus demonstrates the feasibility of an electric field measurement over a wide field strength range of up to 300 V/mm, and more importantly, from Fig. 5(b), the electric field strength down to approximately 0.5 V/mm is detectable at atmospheric pressure.

The relationship between the partial pressure of hydrogen and the square root of the signal intensity is shown in Fig. 6(a) for an applied electric field of 13 V/mm. The signals were averaged over 1000 signals. Herein, to avoid different curvatures of windows causing misalignment of the signal beam, we maintained the total pressure inside the test cell at 1 atm by adding nitrogen molecules. Although we employed a hydrogen and nitrogen mixture, each molecular species has characteristic vibrational and rotational transition energies; therefore, they are seldom confused with each other [32]. In Fig. 6(a), there is an approximate proportionality between the square roots of the measured signal intensities and the partial pressure, that is, the number density of hydrogen molecules.

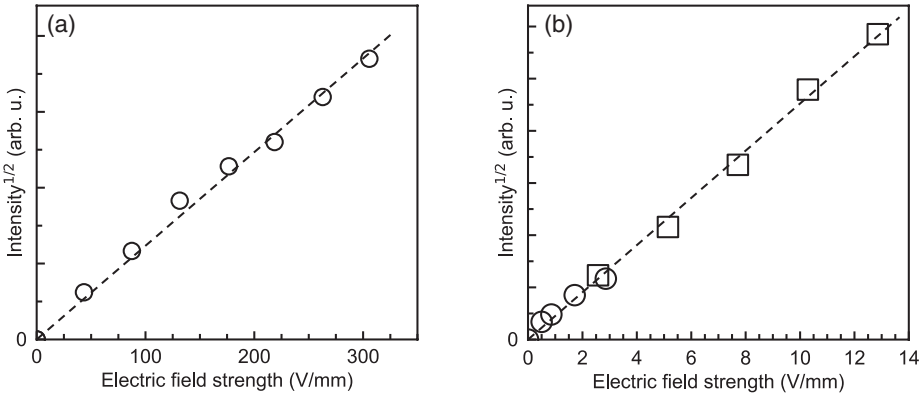

FIG. 5. Square roots of the measured signals as functions of the externally applied electric field strength in hydrogen at 1 atm: (a) strong electric field range of 0–300 V/mm and (b) weak field range of 0–13 V/mm. Three sets of measurements are shown using squares, circles, and diamonds. The broken lines are linear fits to the data. An electric field of approximately 0.5 V/mm was detectable.

This is consistent with the theoretical prediction in Eq. (1); the square root of the CARS intensity is proportional to the number density. In Fig. 6(b), the square roots of the measured signal intensities as functions of the externally applied electric field strength under different partial pressures of hydrogen are shown. For each partial pressure, the square root of the signal intensity is proportional to the electric field strength with different constants of proportionality: the higher the partial pressure, the larger the constant of proportionality. This indicates that it is possible to measure the electric field strength at various pressures and that the higher pressure of the targeted species makes it possible to measure the electric field strength more incisively.

As mentioned above, the minimum detectable field demonstrated is 0.5 V/mm in atmospheric-pressure hydrogen. This value is significantly better than 5 V/mm, which has been demonstrated by conventional E-CARSi [6] and E-FISH [18]. Furthermore, this is the best value in laser-based electric field measurements in atmospheric-pressure environments and even closer to that achieved at low pressure. Additionally, this is the best value even in low-pressure environments in cases without additional probe species, that is, excited or atomic species produced by plasma and discharge. The highly sensitive methods probing the energy shift of Rydberg states of atoms by fluorescence-dip spectroscopy demonstrated 0.3 V/mm for argon [9], 0.5 V/mm for hydrogen [8,17], 2.5 V/mm for krypton [13], and 25 V/mm for xenon [11]. The method that involves argon required metastable argon, which is produced by plasma and discharge, and the method that involved hydrogen required hydrogen atoms, which are also produced by plasma and discharge as the probe, while the ground states of krypton and xenon could be used as the probe atoms. While it is evident that the CARS-based method cannot be sensitive in the low-pressure region [6], and thus, they cannot be compared, the high sensitivity of this simple method, which detects only the intensity of the induced light, is suggested by the fact that the minimum detectable field is the same as that of detecting the energy shift of Rydberg states of atomic hydrogen by fluorescence-dip spectroscopy requiring a wavelength scan [8].

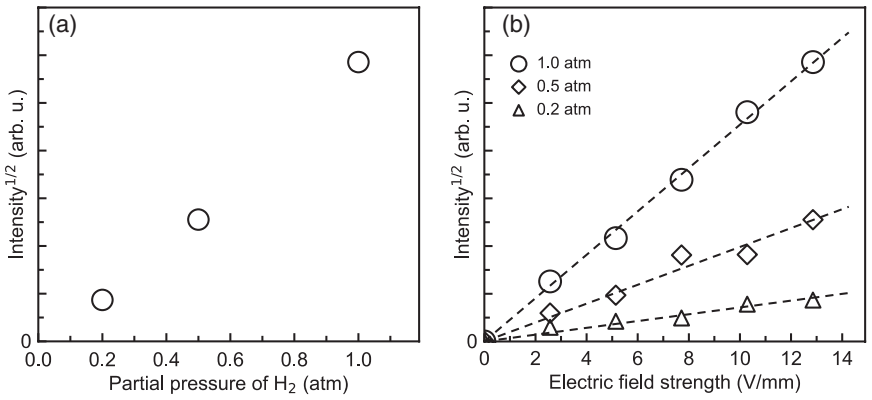

FIG. 6. E-CARSv signal intensities under different hydrogen pressure environments. Square roots of the measured signals as functions of (a) partial pressure of hydrogen and (b) electric field strength for hydrogen partial pressures of 0.2, 0.5, and 1.0 atm. The dotted lines are linear fits to the data of the same pressure.

While the demonstrated 0.5 V/mm detection at atmospheric pressure is already very sensitive, further increasing the sensitivity is possible. First, the narrower linewidth of the laser should enhance the signal intensity, as the linewidth applied in this study was approximately 50 times wider than that of the Raman transition. Second, reducing the laser pulse width τ should also enhance the sensitivity if the linewidth of the laser is kept narrow enough since the signal accumulated over τ is proportional to τ^{-1} in the case modifying τ and keeping the pulse powers (assuming similarity in the pulse shape). For the Gaussian beam, the minimum pulse width fitting within the Doppler broadening of 290 K, thus effectively applied for E-CARSv, should be approximately 400 ps, which is estimated from the minimum linewidth of the Gaussian beam $\Delta\nu_m = 0.44\tau^{-1}$ [33] and the Doppler broadening of 1.1 GHz. Thus, there is room to enhance an order by reducing τ. Another way to increase the sensitivity is to enlarge the focal length as demonstrated in E-FISH [20], while the spatial resolution in the depth direction will be lost. If the electric field is uniformly distributed, the effective interaction length l_i between the laser pulses and electric field should be close to twice the Rayleigh range l_R [20], which was approximately 2 mm in this case. Another length deciding the signal intensity is the coherence length l_c depending on the phase-matching condition. Since there is a wavelength dependence of the refractive index [34,35], there remains a phase mismatch $\Delta k = |k_{\mathrm{CARS}} - k_1 - k_{\mathrm{IR}}|$ with the collinear alignment. As Δk are estimated to be $\sim$0.4 cm^{-1} for pure hydrogen and $\sim$0.5 cm^{-1} for a 20% hydrogen and 80% nitrogen mixture at 1 atm and room temperature, l_c are $\sim$80 and $\sim$60 mm, respectively. For the case $l_c \gg l_i$, the signal quadratically increases with l_i ($C_L \sim l_i^2$). Thus, it is ideally expected that efficient enhancement of the sensitivity in E-CARSv is achieved via increasing l_i (e.g., $\sim$80 mm) with a narrower linewidth (e.g., 1.1 GHz) and short pulse width (e.g., 400 ps) laser, while further detailed discussion may need to also consider the Gouy phase shift [36]. Obtaining such an IR laser might be one of the difficulties of further improving the current E-CARSv.

While high sensitivity has been demonstrated, the disadvantage of E-CARSv is that, to use this method, there are the requirements of finding the molecular density as well as the population in the excited states. This disadvantage also exists with E-FISH, but not with E-CARSi, where the conventional CARS signal can be obtained simultaneously [6]. However, the E-CARSv method can easily estimate the rotational and vibrational temperatures of hydrogen by the population distribution of the Q branches [37], as demonstrated for the rotational states in Fig. 4. The rotational temperature should be nearly in equilibrium with the kinetic temperature [7,32]; thus, we can estimate the molecular density assuming an ideal gas and Boltzmann distribution in rotational states. As vibrationally excited molecules are also detectable, by assuming a Boltzmann distribution for both rotational and vibrational states, we can estimate the specified molecular densities and thus the electric field from the signal intensity. Therefore, without adding new optical equipment, this method supported by an additional wavelength scan should be applicable even for environments, such as plasma environments, where the gaseous temperature or excitation temperatures change. However, if a state is in strong nonequilibrium preventing the assumption of Boltzmann distribution, another method, like conventional Raman scattering with an additional spectrometer, may be required to estimate the molecular density. The proposed method is applicable to media that have Raman-active transitions; therefore, it could be widely applied not only to hydrogen demonstrated in this study but also to nitrogen, which is abundant in the atmosphere.

This work was partially supported by JSPS KAKENHI (Grants No. 16H05988, No. 19H01885, and No. 21H04450). T. I. appreciates the helpful discussions with Professor Cappelli of Stanford University.

*Corresponding author.
tsuyohito@k.u-tokyo.ac.jp

[1] M. J. Rycroft, S. Israelsson, and C. Price, The global atmospheric electric circuit, solar activity and climate change, J. Atmos. Sol. Terr. Phys. **62**, 1563 (2000).
[2] M. J. Rycroft, R. G. Harrison, K. A. Nicoll, and E. A. Mareev, An overview of Earth's global electric circuit and atmospheric conductivity, Space Sci. Rev. **137**, 83 (2008).
[3] D. R. MacGorman and W. D. Rust, *The Electrical Nature of Storms* (Oxford University Press, New York, 1998).
[4] V. E. Shashoua, Static electricity in polymers. I. Theory and measurement, J. Polym. Sci. **33**, 65 (1958).
[5] J. E. Vinson and J. J. Liou, Electrostatic discharge in semiconductor devices: An overview, Proc. IEEE **86**, 399 (1998).
[6] O. A. Evsin, E. B. Kupryanova, V. N. Ochkin, S. Y. Savinov, and S. N. Tskhai, Determination of the intensities of electric fields in gases and plasmas by the CARS method, Quantum Electron. **25**, 278 (1995).
[7] A. N. Goyette, W. B. Jameson, L. W. Anderson, and J. E. Lawler, An experimental comparison of rotational temperature and gas kinetic temperature in a discharge, J. Phys. D **29**, 1197 (1996).
[8] U. Czarnetzki, D. Luggenhölscher, and H. F. Döbele, Sensitive Electric Field Measurement by Fluorescence-Dip Spectroscopy of Rydberg States of Atomic Hydrogen, Phys. Rev. Lett. **81**, 4592 (1998).
[9] K. Takizawa, K. Sasaki, and A. Kono, Sensitive measurements of electric field distributions in low-pressure Ar plasmas by laser-induced fluorescence-dip spectroscopy, Appl. Phys. Lett. **84**, 185 (2004).
[10] C. Tendero, C. Tixier, P. Tristant, J. Desmaison, and P. Leprince, Atmospheric pressure plasmas: A review, Spectrochim. Acta B Atom. Spectros. **61**, 2 (2006).

[11] E. Wagenaars, G. M. W. Kroesen, and M. D. Bowden, Investigations of Stark effects in xenon Rydberg states by laser-induced fluorescence-dip spectroscopy, Phys. Rev. A **74**, 033409 (2006).
[12] M. Gemišić Adamov, A. Steiger, K. Grützmacher, and J. Seidel, Doppler-free Stark spectroscopy of the second excited level of atomic hydrogen for measurements of electric fields, Phys. Rev. A **75**, 013409 (2007).
[13] T. Kampschulte, J. Schulze, D. Luggenhölscher, M. D. Bowden, and U. Czarnetzki, Laser spectroscopic electric field measurement in krypton, New J. Phys. **9**, 18 (2007).
[14] E. Wagenaars, M. D. Bowden, and G. M. W. Kroesen, Measurements of Electric-Field Strengths in Ionization Fronts during Breakdown, Phys. Rev. Lett. **98**, 075002 (2007).
[15] P. J. Bruggeman *et al.*, Plasma-liquid interactions: A review and roadmap, Plasma Sources Sci. Technol. **25**, 053002 (2016).
[16] K.-D. Weltmann and T. von Woedtke, Plasma medicine—current state of research and medical application, Plasma Phys. Controlled Fusion **59**, 014031 (2017).
[17] S. Nishiyama, K. Katayama, H. Nakano, M. Goto, and K. Sasaki, Performance of sheath electric field measurement by saturation spectroscopy in Balmer-α line of atomic hydrogen, Appl. Phys. Express **10**, 036101 (2017).
[18] B. M. Goldberg, T. L. Chng, A. Dogariu, and R. B. Miles, Electric field measurements in a near atmospheric pressure nanosecond pulse discharge with picosecond electric field induced second harmonic generation, Appl. Phys. Lett. **112**, 064102 (2018).
[19] K. H. Burrell, Role of sheared $E \times B$ flow in self-organized, improved confinement states in magnetized plasmas, Phys. Plasmas **27**, 060501 (2020).
[20] A. Dogariu, B. M. Goldberg, S. O'Byrne, and R. B. Miles, Species-Independent Femtosecond Localized Electric Field Measurement, Phys. Rev. Applied **7**, 024024 (2017).
[21] V. N. Ochkin, S. Y. Savinov, S. N. Tskhai, U. Czarnetzki, V. S. von der Gathen, and H. F. Dobele, Nonlinear optical techniques for plasma diagnostics, IEEE Trans. Plasma Sci. **26**, 1502 (1998).
[22] T. Ito, K. Kobayashi, S. Mueller, D. Luggenhölscher, U. Czarnetzki, and S. Hamaguchi, Electric field measurement in an atmospheric or higher pressure gas by coherent Raman scattering of nitrogen, J. Phys. D **42**, 092003 (2009).
[23] W. G. Rado, The nonlinear third order dielectric susceptibility coefficients of gases and optical third harmonic generation, Appl. Phys. Lett. **11**, 123 (1967).
[24] P. R. Régnier and J. P.-E. Taran, On the possibility of measuring gas concentrations by stimulated anti-Stokes scattering, Appl. Phys. Lett. **23**, 240 (1973).
[25] M. A. Buldakov, N. F. Vasil'ev, S. V. Lazarev, and I. I. Matrosov, Determination of the electric field intensity by the coherent anti-stokes Raman spectroscopy method, Sov. J. Quantum Electron. **14**, 278 (1984).
[26] C. F. Kaminski and P. Ewart, Multiplex H_2 coherent anti-Stokes Raman scattering thermometry with a modeless laser, Appl. Opt. **36**, 731 (1997).
[27] W. B. Roh, P. W. Schreiber, and J. P. E. Taran, Single-pulse coherent anti-Stokes Raman scattering, Appl. Phys. Lett. **29**, 174 (1976).
[28] M. A. Woodmansee, R. P. Lucht, and J. C. Dutton, Stark broadening and stimulated Raman pumping in high-resolution N coherent anti-Stokes Raman scattering spectra, AIAA J. **40**, 1078 (2002).
[29] G. Magnotti, A. D. Cutler, G. C. Herring, S. A. Tedder, and P. M. Danehy, Saturation and Stark broadening effects in dual-pump CARS of N_2, O_2, and H_2, J. Raman Spectrosc. **43**, 611 (2012).
[30] C. H. Lui, K. F. Mak, J. Shan, and T. F. Heinz, Ultrafast Photoluminescence from Graphene, Phys. Rev. Lett. **105**, 127404 (2010).
[31] C. Ferrante *et al.*, Raman spectroscopy of graphene under ultrafast laser excitation, Nat. Commun. **9**, 308 (2018).
[32] S. A. J. Druet and J.-P. E. Taran, Cars spectroscopy, Prog. Quantum Electron. **7**, 1 (1981).
[33] A. E. Siegman, *Lasers* (University Science Books, Mill Valley, CA, 1986).
[34] E. R. Peck and B. N. Khanna, Dispersion of nitrogen, J. Opt. Soc. Am. **56**, 1059 (1966).
[35] E. R. Peck and S. Huang, Refractivity and dispersion of hydrogen in the visible and near infrared, J. Opt. Soc. Am. **67**, 1550 (1977).
[36] M. Mansuripur, *Classical Optics and Its Applications* (Cambridge University Press, Cambridge, England, 2002).
[37] W. M. Tolles, J. W. Nibler, J. R. McDonald, and A. B. Harvey, A review of the theory and application of coherent anti-stokes Raman spectroscopy (CARS), Appl. Spectrosc. **31**, 253 (1977).